

Effect of MgO Surface Modification on the TiO₂ Nanowires Electrode for Self-Powered UV Photodetectors

Shiming Ni,[†] Fengyun Guo,^{*,†} Dongbo Wang,^{*,†} Gang Liu,^{*,†,§} Zhikun Xu,^{*,†} Lingping Kong,^{‡,§} Jinzhong Wang,[†] Shujie Jiao,[†] Yong Zhang,[†] Qingjiang Yu,[†] Jiawei Luo,[†] Bao Wang,[†] Zhenghao Li,[†] ChengCheng Zhang,[†] and Liancheng Zhao[†]

[†]Department of Optoelectronic Information Science, School of Materials Science and Engineering, Harbin Institute of Technology, Harbin 150001, China

[‡]Geophysical Laboratory, Carnegie Institution of Washington, Washington, D.C. 20015, United States

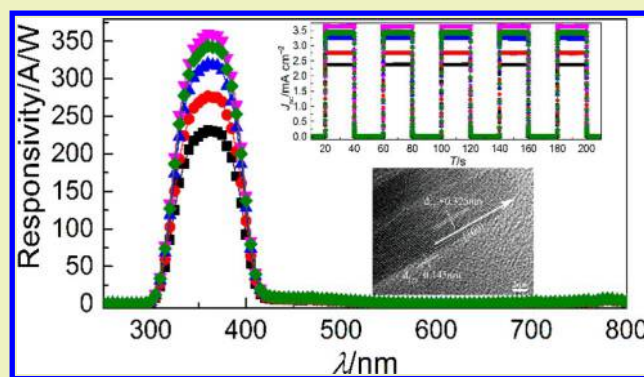
[§]Center for High Pressure Science and Technology Advanced Research, Shanghai 201203, China

[⊥]Key Laboratory for Photonic and Electric Bandgap Materials, Ministry of Education, Harbin Normal University, Harbin 150025, China

Supporting Information

ABSTRACT: TiO₂-based core–shell structure has gained enormous significance and has developed as a promising candidate in photoelectrochemical (PEC) devices due to its excellent properties. Despite studies, the surface/interface chemistry in these nanostructures has not been fully understood and there is still much room to further improve the performance of related PEC devices. Here, using a closely integrated experimental investigation and mechanism analysis, we scrutinized the intrinsic role of the MgO coating in the photocurrent enhancement of TiO₂@MgO core–shell structured UVPDs. We evidenced that after coating with MgO, the photocurrent of UVPDs has been significantly enhanced and the optimal coating time was found to be 45 min. A large responsivity of 365 mA W⁻¹ at 360 nm and a simultaneously excellent on/off ratio of 16 739 are achieved, which have rarely reported previously. In addition, the structure–property relationships are well established in all studied UVPDs through comparing investigations. The superior performance is postulated to be strongly correlated to the suppression of the recombination of photogenerated electron with I₃⁻ in electrolyte. This work sheds some light on searching for new structures for next-generation low cost, large area, and energy-efficient optoelectronic devices.

KEYWORDS: UV photodetector, Coating time, TiO₂@MgO, Nanowires



INTRODUCTION

Currently, TiO₂ nanostructures-based self-powered photoelectrochemical (PEC) UV photodetectors (UVPDs) have attracted great attention due to their chemical inertness, physical stability, high photoconversion efficiency, and photostability.^{1–12} Among all nanostructured counterparts, one-dimensional (1D) nanostructures including nanorods and nanowires are promising in TiO₂-based PEC UVPDs because the grain boundaries are significantly reduced in well crystallized 1D structure, thus providing continuous and highly conductive pathways for the extraction of photogenerated electrons. Consequently, low charge recombination rate and improved charge collection efficiency in these smooth tunnels can be expected.^{13–24} Up to now, a high level of electron conductivity up to 0.1 to 1.0 cm² V⁻¹ S⁻¹, together with stable chemical properties, have been found in rutile TiO₂ nanowires,²⁵ thus making them promising for an active material platform for further UVPD device fabrication.

For PEC UVPDs applications, interfacial charge recombination plays an important role in the device performance. Large interfacial charge recombination can lead to high level loss of photogenerated electrons and low responsivity of the device cannot be avoidable.²⁶ Recently, semiconductor core–shell structures with type-II band alignment have been widely applied photovoltaic devices on account of their high carrier injecting ratio properties and carrier confinement caused by differences in band gap.²⁷ In typical core–shell structures, it is required that the conductive band (CB) of the shell should be positioned above that of the core materials, which builds an energy potential barrier at the photoanode/electrolyte interface. Binary metal oxides such as MgO,²⁸ Ga₂O₃,²⁹ ZrO₂³⁰ and ternary metal oxides such as SrTiO₃³¹ could be potentially

Received: November 15, 2017

Revised: February 4, 2018

Published: May 7, 2018

applied as shell coatings on the surface of TiO_2 . Among these materials, MgO stands out as a competitive material due to its high optical transparency, wide direct band gap, superior chemical inertness, and good thermal stability.³² Currently, several types of MgO/ TiO_2 heterostructures have been applied in dye-sensitized solar cells (DSSCs), photocatalytic, and photowater splitting.^{33–37} However, up to now, the TiO_2 @MgO core–shell structure for self-powered UV photodetectors and their optical response performance are full of challenges and seldom reported, which not only limits our understanding in surface/interface chemistry of TiO_2 -based core–shell structures but also should be paid more attention for further PEC applications from a practical viewpoint.

In this work, we explored the effect of MgO coating on the performance of TiO_2 @MgO core–shell nanowire arrays self-powered UV photodetectors. The diagrammatic structure of the PEC UVPD is shown in Figure 1. A series of TiO_2 @MgO

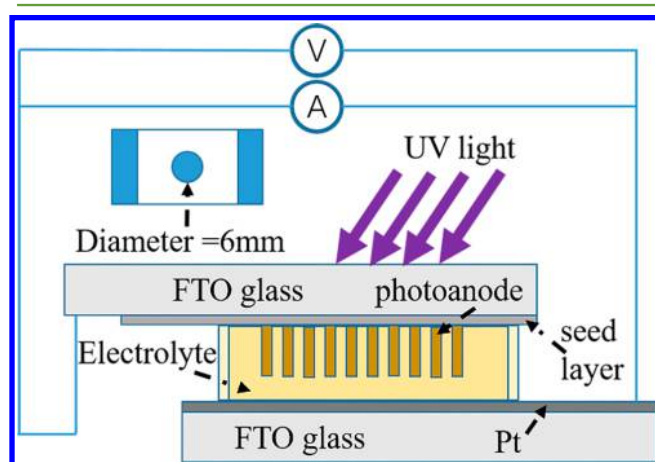


Figure 1. Diagrammatic structure of the PEC UVPD.

core–shell structure nanowire arrays with various shell coating time were fabricated and the respective UVPD device performance were carefully studied. As confirmed from electrochemical, electronic, and spectroscopy characterizations, surprisingly enhanced optical response and photocurrent density were found in designed core–shell structures, which are rooted from the suppression of the recombination of photogenerated electron.

EXPERIMENTAL SECTION

Preparation of TiO_2 Nanowires (NWAs). TiO_2 NWAs were prepared on FTO glass (15Ω square) by a one-step solvothermal method. First, preparation a TiO_2 seed layer on the clean FTO glass by an aqueous solution with 0.2 M TiCl_4 . After maintaining at 70°C for 30 min, the FTO glass was annealing at 550°C for 60 min in air. Subsequently, the FTO glass with seed layer was put in a mixed solution with 3 mL of TiCl_4 , 30 mL of concentrated HCl (36–38 wt %), and 30 mL of ethanol in a 100 mL Teflon-lined stainless steel autoclave. Then, the autoclave was heated at 150°C for 12 h in a constant temperature electric oven. After, the autoclave naturally cooled down to ambient temperature, swilling out the obtained samples with DI water and absolute ethyl alcohol for three times.³⁸

Preparation of TiO_2 @MgO Core–Shell NWAs. Prepared TiO_2 NWAs were immersed into a mixed solution with 25 mL of 0.01 M MgCl_2 and 25 mL of 0.2 M ammonium hydroxide ($\text{NH}_3\cdot\text{H}_2\text{O}$) in the Teflon-lined stainless steel autoclave. The duration of heating was 15, 30, 45, and 60 min, respectively. The alkaline feature of $\text{NH}_3\cdot\text{H}_2\text{O}$ is relatively weak so that the glass cannot be corroded. The obtained bare

rutile TiO_2 NWAs and TiO_2 @MgO core–shell NWAs samples are denoted as T0, T1, T2, T3, and T4, respectively.

Assembling of Photoelectrochemical Self-Powered UVPDs. The as-prepared TiO_2 NWAs and TiO_2 @MgO core–shell NWAs on FTO glass were prepared anodes for photoelectrochemical self-powered UVPDs similar to previous reports.^{39,40} Before assembling, an annealing process at 500°C for 30 min in air is needed for all samples. The solvent of the electrolyte is the mixture of acetonitrile and *n*-Butyl cyanide (volume ratio: 85/15). The concentration of 1,3-dimethylimidazolium, LiI, I_2 , TBP, and guanidinium thiocyanate in the electrolyte is 1.0 M, 0.5 mM, 30 mM, 0.5, and 0.1 M, respectively. A Pt counter electrode was prepared by doctor-blade method with thickness of about $5 \mu\text{m}$. A $60 \mu\text{m}$ thick Bynel film (DuPont) was used as thermal adhesive films between the photoanodes and platinized counter electrodes. An electrolyte-infusing hole was prepared on the corner of the counter electrode and the internal space was filled with a liquid electrolyte by a vacuum backfilling method. Lastly, the electrolyte-infusing hole was sealed hermetically by a cover glass and thermal adhesive films.

Characterization. The choice of X-ray diffraction (XRD) analysis, field emission scanning electron microscopy (FESEM) analysis, and transmission electron microscopy (TEM) and high-resolution TEM (HRTEM) were reported in our previous research.⁴¹ X-ray photoelectron spectroscopy (XPS) measurements of the material binding energy distributions were carried out by the ESCALAB 250Xi spectrometer from Thermo Fisher Scientific. A UV detector (ST-513, UVAB, Sentry Optronics Corp., Taiwan) was used to quantify UV irradiance. A ultraviolet hand lamp with a wavelength of 365 nm was used as the photosource. An Autolab (model AUT84315) electrochemical workstation with a standard three-electrode system was used to examine the J_{sc} - t curves to represent the photoresponse switching behavior of UVPDs. The schematic diagram of the standard three-electrode system is shown in Figure S1. The measurement was conducted at zero bias under the ultraviolet hand lamp with an on/off interval of 20 s. For measuring the wavelength-related photoelectrical response, a xenon lamp with a monochromator used as light source and current signal was measured in short-circuit condition. Meanwhile, a digital power and energy meter (PM100D, Thorlabs) was used to accurate measure UV luminescent intensity in real time. The EIS data of the UVPDs were gathered also by using the Autolab. The EIS measurements were carried out by a bias voltage superposed by a sinusoidal periodic disturbance of 10 mV from 100 kHz to 0.1 Hz in a dark conditions. PL characterizations were recorded in CCD spectroscopy at fixed excitation intensity by a He–Cd laser line of 325 nm at room temperature.

RESULTS AND DISCUSSION

The crystallographic structures of pure TiO_2 (T0) and TiO_2 @MgO core–shell NWAs (T1, T2, T3, T4) were determined by the XRD recorded in the 2θ range of 20° – 80° , and the patterns are shown in Figure 2. For all samples, the peaks located at 62.72° originate from the rutile phase TiO_2 (JCPDS 21-1276). The XRD pattern of the TiO_2 powder that was scratched from

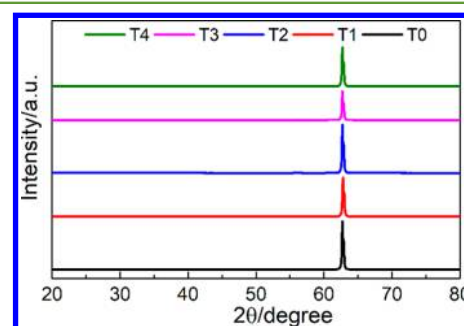


Figure 2. XRD patterns of TiO_2 and TiO_2 @MgO core–shell NWAs.

TiO₂ NWAs (as shown in Figure S2) further confirms the phase composition of the nanowires can be ascribed to the rutile phase. This considering the fact that MgO shell is too thin to be detected by X-ray, it can be easily understood that the Bragg reflections assigned by MgO in the XRD pattern was not observed.

The properties of nanomaterials are strongly related to their micro morphology. FESEM measurements give us the morphology of TiO₂ and TiO₂@MgO NWAs (T4), as shown in Figure S3. Clearly, the analyzed TiO₂ nanowire arrays exhibit a high uniformity, with average diameters of ~ 15 nm and length of ~ 30 μm . Furthermore, we conclude that there is no obvious difference in the morphology between the pure TiO₂ NWAs and MgO coated ones. The EDS results (as shown in Figure S4) show that as expected the Mg element content increases when prolonging the MgO coating time (detailed information listed in Table S1). The results of XPS also confirm this conclusion (shown in Figure S5). To investigate the elemental distribution of TiO₂@MgO core-shell NWAs, element-mapping characterization is performed on T4 sample, which is also obtained from EDS. Figure S6 shows the image of each element corresponding to Mg, O, and Ti, respectively, and implies that all elements are homogeneously distributed on the top-surface area of the TiO₂@MgO core-shell NWAs. As shown in Figure S7, to compare between the distribution of Mg element of T4 and the sample whose MgO treatment time is 120 min, we find that the increase of Mg content detected by EDS is the result of the larger coated MgO area. Integrating the FESEM results, we postulate that the variation of coating time changes the coating area.

Details about microstructures of TiO₂@MgO core-shell NWAs were investigated by TEM and HRTEM. The microstructure of T4 is shown in Figure 3a, in which one can

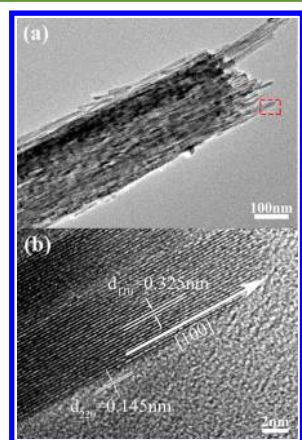


Figure 3. Structural characterizations of TiO₂@MgO core-shell NWAs: (a) TEM image of TiO₂@MgO core-shell NWAs; (b) HRTEM image of a single TiO₂@MgO core-shell NW.

see the porous structure that is very useful for electrolyte penetrating in PEC UVPDs. Further insight into the microstructure of a single TiO₂@MgO core-shell nanowire is revealed by the typical HRTEM lattice image (Figure 3b). The clear lattice fringes of both TiO₂ and MgO can be distinguished from the HRTEM image. The interplanar spacing of ~ 0.325 nm is well corresponding to the {110} planes of rutile TiO₂, indicating that the growth direction of TiO₂ NWs is along the [001] direction.⁴¹ The interplanar spacing with ~ 0.145 nm is in good accordance with that of the (220) plane of cubic MgO,⁴²

demonstrating the formation of a TiO₂@MgO heterostructure. The thickness of the MgO shell of all samples is about 2 nm.

The samples obtained at different coating treatments were then exploited as photoanodes to assemble PEC UVPDs and the device performance are fully characterized. The photoelectricity response of T0–T4 based self-powered UVPDs is shown in Figure 4a. We observed that the J signal can be

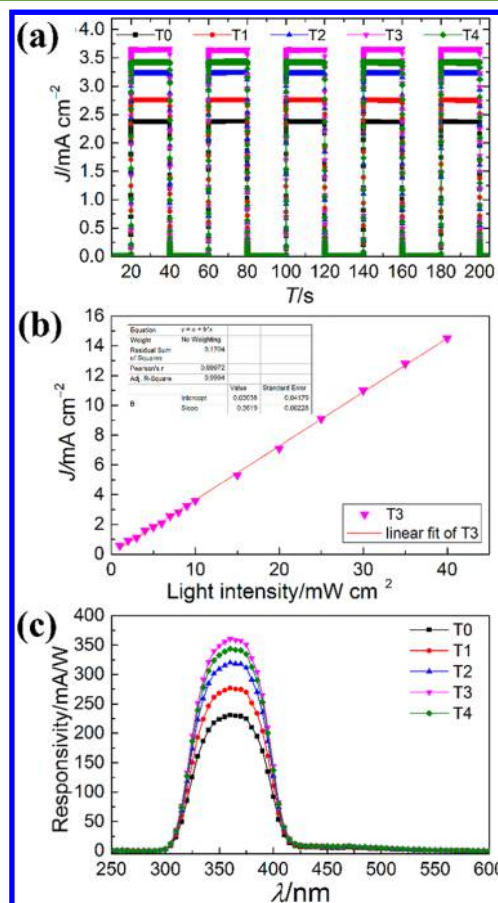
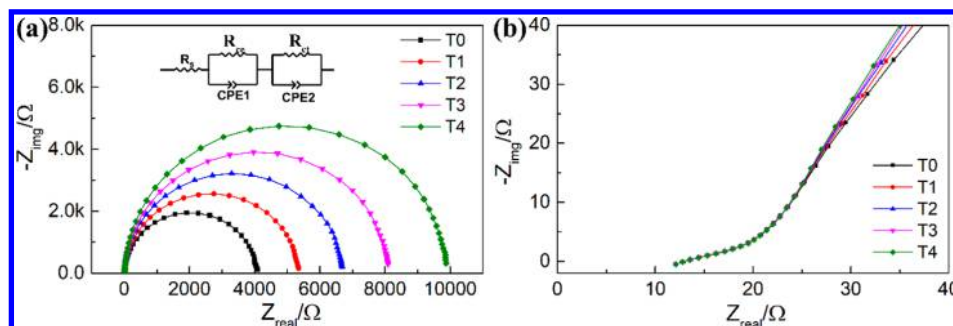


Figure 4. (a) Photocurrent responses of UVPDs under on/off radiation of 10 mW cm^{-2} UV light illumination ($\lambda = 365 \text{ nm}$); (b) J as a function of the incident UV light intensity from 1 to 40 mW cm^{-2} for the UVPD based on T3; (c) responsivity spectra of based UVPDs.

reproducibly switched from the “on” state to the “off” state by periodically turning the UV light on and off with a light density of 10 mW cm^{-2} for all UVPDs, indicating that all UVPDs have good stability. It is worth noting that compared with bare TiO₂ nanowire arrays, the photocurrent of UVPDs has been significantly enhanced after coating with MgO, even undergoing the shortest coating time (T1). As the coating time increases from 0 to 45 min, photocurrent density (J_{sc}) sharply increases from 0 to 3.60 mA cm^{-2} , followed by a significant decrease to 3.43 mA cm^{-2} if the coating time is further increased to 60 min. Simultaneously, as shown in Figure S8, the dark current first decreases as coating time is prolonged to 45 min and then increases for the case of 60 min coating time. The photoresponse sensitivity, named on/off ratio, is defined as $(J_{\text{light}} - J_{\text{dark}})/J_{\text{dark}}$.⁴³ With the increasing of coating time from 0 to 45 min, the on/off ratio rises sharply and reaches a maximum of 16 739. Response time is usually represented by the rise time (τ_r) and decay time (τ_d) of all UVPDs, which could be observed from the enlarged rising and recovering edge of the

Table 1. Performance Characteristics including J_{sc} , J_{dark} , On/Off Ratio, and R_λ of UVPDs

Sample	T0	T1	T2	T3	T4
J_{sc} (mA cm ⁻²)	2.38 ± 0.02	2.76 ± 0.02	3.23 ± 0.02	3.60 ± 0.02	3.43 ± 0.02
J_{dark} (μA cm ⁻²)	0.27831 ± 0.002	0.25029 ± 0.002	0.22421 ± 0.002	0.21507 ± 0.002	0.23642 ± 0.002
On/off ratio	8552 ± 5	11027 ± 5	14407 ± 5	16739 ± 5	14509 ± 5
R_λ (mA W ⁻¹)	240 ± 0.5	278 ± 0.5	320 ± 0.5	365 ± 0.5	340 ± 0.5

**Figure 5.** (a) Nyquist plots of EIS data for all UVPDs at a 0.5 V bias; (b) enlarged tiny semicircle in the higher-frequency range.

periodically photoelectricity response in Figure S9. The τ_r is usually defined as the time to increase from 0 to $1-1/e$ of the maximum photocurrent, and the τ_d is the time to recovery to $1/e$ of the maximum photocurrent. The τ_r of all the UVPDs is very close to one another.⁴³ However, the existence of MgO would increase the τ_d , which suggests that the electron recombination at the NWAs/electrolyte interface can be restrained by the MgO shell. The detailed data are shown in Table S2.

In addition, the dependence of J_{sc} on incident light intensity is another significant property for UVPDs. Figure 4b and Figure S10 show the relationship between the J_{sc} of all UVPDs and the intensities of incident light. The J_{sc} measurements of UVPDs were carried out under a 365 nm UV light source whose light intensity varied from 1 to 40 mW cm⁻². The slope of data is fitted through linear approximation by the least-square method. The linear fitting result shows a significant linear dependence of the photocurrent on the irradiation intensity in a wide range, indicating that this type of photodetector could be applied for precise UV light intensity measurement. To test the spectral responsivity of the UVPDs, the wavelength selective property was measured in terms of the current signal in the range of 250–600 nm at a zero bias, and the results are shown in Figure 4c. Photoresponsivity (R_λ) is an important property for photodetector performance, which can directly affect the final device spectral response. For all UVPDs, all the R_λ peaks are at 360 nm. However, as can be seen in Figure 4c, the maximum value of R_λ for a bare TiO₂ NWAs-based UVPD is approximately 240 mA W⁻¹. Meanwhile, the peak R_λ of UVPD based on T3 is approximately 365 mA W⁻¹. More importantly, consistent with photocurrent results, the R_λ changes drastically with the coating time variation. What is more, the R_λ matches the slope gotten from the fitting results of the relationship between J_{sc} values and the incident light intensities. At present, the highest photoresponse of PEC UVPDs based on TiO₂ nanowire/nanobranh arrays is 220 mA W⁻¹.^{43–45} It is noted that the UVPD based on TiO₂@MgO core-shell NWAs exhibits a higher photosensitivity with those reported by other authors, and the corresponding information is shown in Table S3. The detailed data about the short-circuit current density (J_{sc}), on/off ratio, and R_λ are listed in Table 1.

To explore the mechanism of enhanced photoresponse performance discussed above, the electron collection efficiency varied with the coating time has been studied by using various characterization techniques including optical absorbance test, electrochemical impedance spectroscopy (EIS), as well as photoluminescence (PL) measurement.

Factors affecting photoresponse performance of the PEC UVPDs mainly include light harvesting efficiency and electron collection efficiency.^{5,46} As shown in Figure S11, the reflection of all different photoanodes is very close to one another, concluding that the extremely thin MgO shell (2 nm) may not influence the light absorption of TiO₂ NWAs at a range of wavelength from 300 to 400 nm.

The electron collection efficiency is related to electron transport efficiency in photoanode and ratio of electron recombination at the interface of photoanode/electrolyte.⁴⁷ Enhancing the electron transmission speed or reducing photogenerated electron recombination at the interface of photoanode/electrolyte both could improve the performance of PEC UVPDs.⁴³ In this case, we introduced the electrochemical impedance spectroscopy (EIS) analysis to clarify the effect of MgO coating on the electron transmission speed and interfacial photogenerated electron recombination.^{48–50} An equivalent circuit (inset in Figure 5a) was applied to fit the Nyquist plots to estimate the sheet resistance (R_s) and charge transfer resistance (R_{ce} and R_{ct}). Commonly, there are two semicircles in the Nyquist plots. The tiny semicircle in the higher-frequency range (as shown in Figure 5b) describes the impedance at the counter electrode/electrolyte interface related to the redox reactions (R_{ce}). The bigger semicircle in the midfrequency range represents the impedance corresponding to the charge recombination process at the photoanode/electrolyte interface (R_{ct}).^{51,52} Figure 5 shows the Nyquist plots of all UVPDs under a bias of 0.5 V in dark conditions, from which the series resistance R_s and charge recombination resistance R_{ct} can be obtained through fitting the Nyquist curves.^{53,54} Considering that the magnitude of the R_s can be qualitatively compared with the electron transmission speed of the charge in the photoanode and the fact that the series resistances of all devices are almost the same, we demonstrate here that the coating of MgO has little effect on the transmission of electrons.^{55,56} Meanwhile, with the increase-

ment of coating time we witness the augment of the of R_{ct} magnitude, which indicates that the increment of the coating area would be ascribed to the inhibition of recombination between photogenerated electron and the I_3^- in the photoanode/electrolyte interface. Detailed data of R_s and R_{ct} are shown in Table S4.

In order to further elaborate the mechanism of MgO coating on the charge recombination, we give a simple energy-band diagram to show the working principles for the PEC UVPD (see Figure 6). The band gap of MgO is about 7.83 eV, and

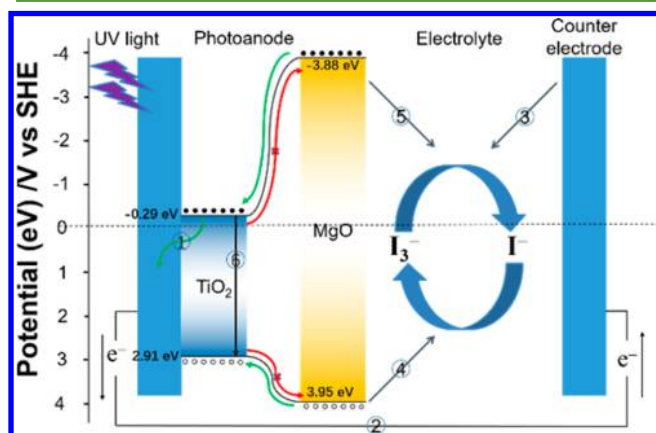


Figure 6. Sketch map of the energy band structure of $TiO_2@MgO$ core-shell structure and the photoinduced charge separation and transfer at the interface of photoanode/electrolyte.

much larger than that of rutile TiO_2 (3.2 eV),⁵⁷ so there is not enough energy for the electron transition from the valence band (VB) to conduction band (CB) by the light source used in this experiment. When UV light shines on the UVPD, the incident photons pass through the FTO glass into the TiO_2 active layer, and then the electron-hole pairs generate in the TiO_2 . As a result, parts of the photogenerated electrons will diffuse through the TiO_2 nanowires and reach the FTO glass (course 1 in Figure 6), and then reach the counter electrode through the external circuit (course 2 in Figure 6). Inevitably, I_3^- in electrolyte will react with these electrons and I^- will be generated (course 3 in Figure 6). Then, the photogenerated holes transmit to the photoanode/electrolyte interface and trap I^- in the electrolyte, and the trapped I^- will be oxidized into I_3^- (course 4 in Figure 6).¹ These reactions complete the circuit. However, parts of photogenerated electrons will be trapped by oxidizing I_3^- at the photoanode/electrolyte interface (course 5 in Figure 6), and will be directly recombined by the photogenerated hole (course 6 in Figure 6). As shown in Figure 6, the CB potential of the MgO is more negative than that of the TiO_2 , which will form a matched bandgap energy structure at the semiconductor/electrolyte interface.⁵⁸ This established energy barrier gotten from the energy structure is favored in the process of the separation of photogenerated electron-hole pairs and thus suppresses the recombination of photogenerated electron with I_3^- in electrolyte, thereby improving the current density of UV detectors.²⁷ This can well explain that when the coating time increases from 0 to 45 min, the current density increases with the coating time.

In the meantime, the VB of MgO is more positive than that of TiO_2 , which would also inhibit photogenerated holes reacting with the I^- in electrolyte. This inhibition will induce the augment of the recombination of photogenerated electron

and holes, which would decrease the current density. Normally, the carrier recombination always results in luminescence emission, so the separation property of the photogenerated electron-hole pairs can be assessed by the emission intensity in the photoluminescence (PL) spectrum.⁵⁹ As shown in Figure 7, the

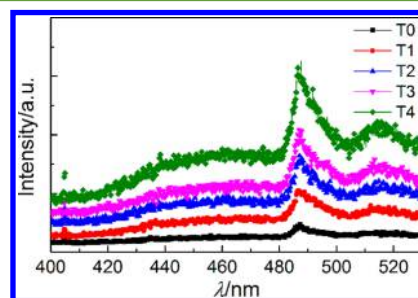


Figure 7. PL spectra measured at room temperature of all samples on FTO substrates.

augment of the emission intensity of the PL spectra, which have been performed on all samples, indicates that the recombination of the photogenerated electron-hole pair at the optical anode is constantly enhanced.⁶⁰

As same as DSCs, the electron lifetime (τ_n) is a key evaluation criterion that determines the recombination dynamics of photogenerated electrons in PEC UVPDs.⁵² The enhancement of the τ_n means the obvious reduction of the electron recombination. A lower electron recombination rate is closely related to a higher charge-collection efficiency, which will bring about larger J_{sc} and smaller dark current intensity as well as on/off ratio. The τ_n values of photoelectrons in NWA films can also be obtained according to the EIS analysis.² The Bode phase plots (frequency vs phase angle) of the EIS results for the above all UVPDs are shown in Figure 8a. The τ_n in the

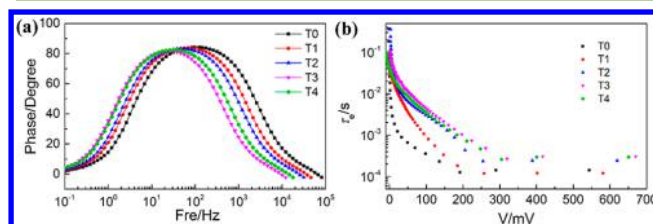


Figure 8. (a) Bode phase plots for all UVPDs at a 0.5 V bias; (b) τ_e (in log-linear representation) as a function of open-circuit voltage.

oxide film can be estimated from the characteristic frequencies (f_{max}) of the impedance semicircle at middle frequencies according to the relation $\tau_n = 1/(2\pi f_{max})$. Detailed data of τ_n are shown in Table S4. The change law of the electron lifetime is consistent with the variation of the current density.

To identify the exciton lifetime (τ_e) of all UVPDs more accurately, open-circuit voltage decay (OCVD) measurement was carried out. The τ_e can be calculated from the representative voltage decay curves of the devices (Figure S12), and the equation we used could be found in other literature.^{54,61,62} The τ_e (in log-linear representation) as a function of V_{oc} is illustrated in Figure 8b, and the τ_e trend is consistent with the EIS analysis.

The R_{ct} of the T3-based UVPD is lower than that of the T4-based UVPDs, but the τ_n (or τ_e) of photoelectrons in the T3-based UVPD is longer than that of photoelectrons in T4-based UVPDs at a given bias. This experimental phenomenon

demonstrates that when the coating time is too long (such as 60 min), the effect of promotion of the recombination of photogenerated electrons and holes on τ_n is more than that of suppressing the recombination of photogenerated electron with I_3^- in electrolyte.

CONCLUSION

In conclusion, we explored the effect of MgO coating on the performance of TiO₂@MgO core-shell nanowire arrays self-powered UV photodetectors that have been designed and fabricated in an economically efficient and environmentally friendly manner. The properties of the TiO₂@MgO heterojunction and the UVPDs device performance have been carefully investigated by using various experimental methods, and a mechanism-related model has been developed. Compared with pure TiO₂ nanowire arrays, the photocurrent of UVPDs has been significantly enhanced after coating with MgO. The UVPDs with a coating time of 45 min exhibited more excellent photoresponse properties than other TiO₂@MgO core-shell structured UVPDs. A large responsivity located at 360 nm of 360 mA W⁻¹ was achieved for the UVPD with MgO shell (coating 45 min) without applied bias together with the excellent on/off ratio of 16 739. All these suggest that this novel UV photodetector is a prospective option as a next-generation low-cost, large area, and energy-efficient optoelectronic UVPD for practical applications.

ASSOCIATED CONTENT

Supporting Information

The Supporting Information is available free of charge on the ACS Publications website at DOI: 10.1021/acssuschemeng.7b04188.

XRD patterns of TiO₂ powders; morphological characterizations of TiO₂ and TiO₂@MgO core-shell NWAs (T4); EDS spectra and XPS result of the TiO₂@MgO NWAs grown on FTO substrate; EDS element mapping of element of T4; current intensity as a function of the incident UV light intensity from 1 to 40 mW cm⁻² for the TiO₂@MgO NWAs-based UVPD; dark current density-voltage of all UVPDs; enlarged rising and decaying edges of the photocurrent response for all UVPDs; UV-vis light reflection spectra, open-circuit voltage decay for all UVPDs; content of Mg element in TiO₂@MgO NWAs with different treatment times; τ_r and τ_d of UVPDs R_i of photoelectrochemical self-powered UVPDs based on various TiO₂ nanostructures; detailed data about series resistance, charge recombination resistance, and electron (PDF)

AUTHOR INFORMATION

Corresponding Authors

*E-mail: guowen@hit.edu.cn (Fengyun Guo).

*E-mail: wangdongbo@hit.edu.cn (Dongbo Wang).

*E-mail: hit071202@gmail.com (Gang Liu).

*E-mail: xuzhikunnano@163.com (Zhikun Xu).

ORCID

Dongbo Wang: 0000-0001-6058-9660

Yong Zhang: 0000-0002-9587-4039

Qingjiang Yu: 0000-0002-9517-1878

Author Contributions

Fengyun Guo and Gang Liu conceived the idea and designed the experiments; Zhikun Xu, Bao Wang, Chuanyang Luan, Zhenghao Li, and Lingping Kong performed the experiments; Dongbo Wang, Jingzhong Wang, Qingjiang Yu, Liancheng Zhao, and Shiming Ni analyzed the data; Dongbo Wang and Shiming Ni wrote the paper.

Funding

This work was supported by the National Natural Science Foundation of China under the contract No. 51502061 and 61605036.

Notes

The authors declare no competing financial interest.

ACKNOWLEDGMENTS

This work was supported by the National Natural Science Foundation of China under the contract No. 51502061 and 61605036.

REFERENCES

- (1) Li, X.; Gao, C.; Duan, H.; Lu, B.; Pan, X.; Xie, E. Nanocrystalline TiO₂ film based photoelectrochemical cell as self-powered UV-photodetector. *Nano Energy* **2012**, *1* (4), 640.
- (2) Hu, B.; Tang, Q.; He, B.; Lin, L.; Chen, H. Mesoporous TiO₂ anodes for efficient dye-sensitized solar cells: an efficiency of 9.86% under one sun illumination. *J. Power Sources* **2014**, *267*, 445.
- (3) Li, X.; Gao, C.; Duan, H.; Lu, B.; Wang, Y.; Chen, L.; Zhang, Z.; Pan, X.; Xie, E. High-performance photoelectrochemical-type self-powered UV photodetector using epitaxial TiO₂/SnO₂ branched heterojunction nanostructure. *Small* **2003**, *9* (11), 2005.
- (4) Xie, Y.; Wei, L.; Li, Q.; Chen, Y.; Liu, H.; Yan, S.; Jiao, J.; Liu, G.; Mei, L. A high performance quasi-solid-state self-powered UV photodetector based on TiO₂ nanorod arrays. *Nanoscale* **2014**, *6* (15), 9116.
- (5) Wang, Z.; Ran, S.; Liu, B.; Chen, D.; Shen, G. Multilayer TiO₂ nanorod cloth/nanorod array electrode for dye-sensitized solar cells and self-powered UV detectors. *Nanoscale* **2012**, *4* (11), 3350.
- (6) Cheng, P.; Liu, Y.; Sun, P.; Du, S.; Cai, Y.; Liu, F.; Zheng, J.; Lu, G. Hydrothermally growth of novel hierarchical structures titanium dioxide for high efficiency dye-sensitized solar cells. *J. Power Sources* **2014**, *268*, 19.
- (7) Han, Y.; Fan, C.; Wu, G.; Chen, H.; Wang, M. Low-temperature solution processed ultraviolet photodetector based on an ordered TiO₂ nanorod array-polymer hybrid. *J. Phys. Chem. C* **2011**, *115* (27), 13438.
- (8) Lee, W. J.; Hon, M. H. An ultraviolet photo-detector based on TiO₂/water solid-liquid heterojunction. *Appl. Phys. Lett.* **2011**, *99* (25), 251102.
- (9) Cao, C.; Hu, C.; Wang, X.; Wang, S.; Tian, Y.; Zhang, H. UV sensor based on TiO₂ nanorod arrays on FTO thin film. *Sens. Actuators, B* **2011**, *156* (1), 114.
- (10) Wang, Y.; Han, W.; Zhao, B.; Chen, L.; Teng, F.; Li, X.; Gao, C.; Zhou, J.; Xie, E. Performance optimization of self-powered ultraviolet detectors based on photoelectrochemical reaction by utilizing dendriform titanium dioxide nanowires as photoanode. *Sol. Energy Mater. Sol. Cells* **2015**, *140*, 376.
- (11) Kim, C. W.; Suh, S. P.; Choi, M. J.; Kang, Y. S.; Kang, Y. S. Fabrication of SrTiO₃-TiO₂ heterojunction photoanode with enlarged pore diameter for dye-sensitized solar cells. *J. Mater. Chem. A* **2013**, *1* (38), 11820.
- (12) Zhao, L.; Zhong, C.; Wang, Y.; Wang, S.; Dong, B.; Wan, L. Ag nanoparticle-decorated 3D flower-like TiO₂ hierarchical microstructures composed of ultrathin nanosheets and enhanced photoelectrical conversion properties in dye-sensitized solar cells. *J. Power Sources* **2015**, *292*, 49.

- (13) Nelson, J. Continuous-Time random-walk model of electron transport in nanocrystalline TiO₂ electrodes. *Phys. Rev. B: Condens. Matter Mater. Phys.* **1999**, *59* (23), 15374.
- (14) Fisher, A. C.; Peter, L. M.; Ponomarev, E. A.; Walker, A. B.; Wijayantha, K. G. U. Intensity dependence of the back reaction and transport of electrons in dye-sensitized nanocrystalline TiO₂ solar cells. *J. Phys. Chem. B* **2000**, *104* (5), 949.
- (15) Law, M.; Greene, L. E.; Johnson, J.; Saykally, C. R.; Yang, P. D. Nanowire dye-sensitized solar cells. *Nat. Mater.* **2005**, *4* (6), 455.
- (16) Jang, Y. H.; Xin, X.; Byun, M.; Jang, Y. J.; Lin, Z.; Kim, D. H. An unconventional route to high-efficiency dye-sensitized solar cells via embedding graphitic thin films into TiO₂ nanoparticle photoanode. *Nano Lett.* **2012**, *12* (1), 479.
- (17) Peng, X. S.; Chen, A. C. Large-scale synthesis and characterization of TiO₂-based nanostructures on Ti substrates. *Adv. Funct. Mater.* **2006**, *16* (10), 1355.
- (18) Liang, J.; Zhang, G.; Yin, J.; Yang, Y. Transparent, 3-dimensional light-collected, and flexible fiber-type dye-sensitized solar cells based on highly ordered hierarchical anatase TiO₂ nanorod arrays. *J. Power Sources* **2014**, *272*, 719.
- (19) Poudel, P.; Qiao, Q. One dimensional nanostructure/nanoparticle composites as photoanodes for dye-sensitized solar cells. *Nanoscale* **2012**, *4* (9), 2826.
- (20) Wang, J.; Lin, Z. Dye-sensitized TiO₂ nanotube solar cells: atomic structural and surface engineering on TiO₂ nanotubes. *Chem. - Asian J.* **2012**, *7* (12), 2754.
- (21) Zhao, J.; Yao, J.; Zhang, Y.; Guli, M.; Xiao, L. Effect of thermal treatment on TiO₂ nanorod electrodes prepared by the solvothermal method for dye-sensitized solar cells: Surface reconfiguration and improved electron transport. *J. Power Sources* **2014**, *255*, 16.
- (22) Wang, J.; Lin, Z. Anodic formation of ordered TiO₂ nanotube arrays: effects of electrolyte temperature and anodization potential. *J. Phys. Chem. C* **2009**, *113* (10), 4026.
- (23) Wang, J.; Lin, Z. Dye-sensitized TiO₂ nanotube solar cells with markedly enhanced performance via rational surface engineering. *Chem. Mater.* **2010**, *22* (2), 579.
- (24) Wang, J.; Lin, Z. Freestanding TiO₂ nanotube arrays with ultrahigh aspect ratio via electrochemical anodization. *Chem. Mater.* **2008**, *20* (4), 1257.
- (25) Liu, B.; Aydil, E. S. Growth of oriented single-crystalline rutile TiO₂ nanorods on transparent conducting substrates for dye-sensitized solar cells. *J. Am. Chem. Soc.* **2009**, *131* (11), 3985.
- (26) Zhang, Q.; Cao, G. Nanostructured photoelectrodes for dye-sensitized solar cells. *Nano Today* **2011**, *6* (1), 91.
- (27) Selinsky, R. S.; Ding, Q.; Faber, M. S.; Wright, J. C.; Jin, S. Quantum dot nanoscale heterostructures for solar energy conversion. *Chem. Soc. Rev.* **2013**, *42* (7), 2963.
- (28) Yuasa, S.; Nagahama, T.; Fukushima, A.; Suzuki, Y.; Ando, K. Giant room-temperature magnetoresistance in single-crystal Fe/MgO/Fe magnetic tunnel junctions. *Nat. Mater.* **2004**, *3*, 868.
- (29) Sun, X.; Li, Y. Ga₂O₃ and GaN semiconductor hollow spheres. *Angew. Chem., Int. Ed.* **2004**, *43* (29), 3827.
- (30) Liu, B.; Zhao, X.; Terashima, C.; Fujishima, A.; Nakata, K. Thermodynamic and kinetic analysis of heterogeneous photocatalysis for semiconductor systems. *Phys. Chem. Chem. Phys.* **2014**, *16* (19), 8751.
- (31) Yang, Y.; Hou, J.; Xing, B.; Zhang, F.; Tian, X.; Yang, H.; Yang, H. G. Ultrathin SnO₂ scaffolds for TiO₂-based heterojunction photoanodes in dye-sensitized solar cells: oriented charge transport and improved light scattering. *Chem. - Eur. J.* **2013**, *19* (28), 9366.
- (32) Gao, D. Z.; Watkins, M. B.; Shluger, A. L. Transient mobility mechanisms of deposited metal atoms on insulating surfaces: Pd on MgO(100). *J. Phys. Chem. C* **2012**, *116* (27), 14471.
- (33) Kulkarni, A.; Jena, A. K.; Chen, H.-W.; Sanehira, Y.; Ikegami, M.; Miyasaka, T. Revealing and reducing the possible recombination loss within TiO₂ compact layer by incorporating MgO layer in perovskite solar cells. *Sol. Energy* **2016**, *136*, 379.
- (34) Wu, S.; Han, H.; Tai, Q.; Zhang, J.; Xu, S.; Zhou, C.; Yang, Y.; Hu, H.; Chen, B.; Sebo, B.; Zhao, X.-Z. Enhancement in dye-sensitized solar cells based on MgO-coated TiO₂ electrodes by reactive DC magnetron sputtering. *Nanotechnology* **2008**, *19* (21), 215704.
- (35) Jung, H. S.; Lee, J. K.; Nastasi, M.; Lee, S.-W.; Kim, J.-Y.; Park, J.-S.; Hong, K. S.; Shin, H. Preparation of nanoporous MgO-coated TiO₂ nanoparticles and their application to the electrode of dye-sensitized solar cells. *Langmuir* **2005**, *21* (23), 10332.
- (36) Bandara, J.; Kuruppu, S. S.; Pradeep, U. W. The promoting effect of MgO layer in sensitized photodegradation of colorants on TiO₂/MgO composite oxide. *Colloids Surf., A* **2006**, *276* (1–3), 197.
- (37) López, T.; Hernández, J.; Gomez, R.; Bokhimi, X.; Boldú, J. L.; Muñoz, E.; Novaro, O.; García-Ruiz, A. Synthesis and characterization of TiO₂-MgO mixed oxides prepared by the sol-gel method. *Langmuir* **1999**, *15* (18), 5689.
- (38) Li, H.; Yu, Q.; Huang, Y.; Yu, C.; Li, R.; Wang, J.; Guo, F.; Jiao, S.; Gao, S.; Zhang, Y.; Zhang, X.; Wang, P.; Zhao, L. Ultralong rutile TiO₂ nanowire arrays for highly efficient dye-sensitized solar cells. *ACS Appl. Mater. Interfaces* **2016**, *8* (21), 13384.
- (39) Yu, Q.; Yu, C.; Guo, F.; Wang, J.; Jiao, S.; Gao, S.; Li, H.; Zhao, L. A stable and efficient quasi-solid-state dye-sensitized solar cell with a low molecular weight organic gelator. *Energy Environ. Sci.* **2012**, *5* (3), 6151.
- (40) Li, X.; Yu, Q.; Yu, C.; Huang, Y.; Li, R.; Wang, J.; Guo, F.; Zhang, Y.; Gao, S.; Zhao, L. Zinc-doped SnO₂ nanocrystals as photoanode materials for highly efficient dye-sensitized solar cells. *J. Mater. Chem. A* **2015**, *3* (15), 8076.
- (41) Huang, Y.; Yu, Q.; Wang, J.; Li, X.; Yan, Y.; Gao, S.; Shi, F.; Wang, D.; Yu, C. A high-performance self-powered UV photodetector based on SnO₂ mesoporous spheres@TiO₂. *Electron. Mater. Lett.* **2015**, *11* (6), 1059.
- (42) Stampe, P. A.; Kennedy, R. J. Growth of MgO on Si (100) and GaAs (100) by laser ablation. *Thin Solid Films* **1998**, *326* (1–2), 63.
- (43) Zhou, J.; Chen, L.; Wang, Y.; He, Y.; Pan, X.; Xie, E. An overview on emerging photoelectrochemical self-powered ultraviolet photodetectors. *Nanoscale* **2016**, *8* (1), 50.
- (44) Xie, Y.; Wei, L.; Li, Q.; Chen, Y.; Yan, S.; Jiao, J.; Liu, G.; Mei, L. High-performance self-powered UV photodetectors based on TiO₂ nano-branched arrays. *Nanotechnology* **2014**, *25* (7), 075202.
- (45) Xie, Y.; Wei, L.; Wei, G.; Li, Q.; Wang, D.; Chen, Y.; Yan, S.; Liu, G.; Mei, L.; Jiao, J. A self-powered UV photodetector based on TiO₂ nanorod arrays. *Nanoscale Res. Lett.* **2013**, *8* (1), 188.
- (46) Zhou, Z.; Fan, J.; Wang, X.; Zhou, W.; Du, Z.; Wu, S. Effect of highly ordered single-crystalline TiO₂ nanowire length on the photovoltaic performance of dye-sensitized solar cells. *ACS Appl. Mater. Interfaces* **2011**, *3* (11), 4349.
- (47) Grätzel, M. Photoelectrochemical cells. *Nature* **2001**, *414*, 338.
- (48) Bisquert, J. Theory of the impedance of electron diffusion and recombination in a thin layer. *J. Phys. Chem. B* **2002**, *106* (2), 325.
- (49) Wang, Q.; Ito, S.; Grätzel, M.; Fabregat-Santiago, F.; Mora-Seró, I.; Bisquert, J.; Bessho, T.; Imai, H. Characteristics of high efficiency dye-sensitized solar cells. *J. Phys. Chem. B* **2006**, *110* (50), 25210.
- (50) Bisquert, J.; Fabregat-Santiago, F.; Mora-Seró, I.; Garcia-Belmonte, G.; Giménez, S. Electron lifetime in dye-sensitized solar cells: theory and interpretation of measurements. *J. Phys. Chem. C* **2009**, *113* (40), 17278.
- (51) Nayak, J.; Prabakar, K.; Park, J. W.; Kim, H. Effect of synthesis temperature on structure, optical and photovoltaic properties of TiO₂ nanorod thin films. *Electrochim. Acta* **2012**, *65*, 44.
- (52) Liu, Y.; Zhang, M.; Jiang, Y.; Xia, Y.; Sun, W.; Zhao, X. General strategy to construct hierarchical TiO₂ nanorod arrays coupling with plasmonic resonance for dye-sensitized solar cells. *Electrochim. Acta* **2015**, *173*, 483.
- (53) Wu, W.; Xu, Y.; Rao, H.; Su, C.; Kuang, D. Multistack integration of three-dimensional hyperbranched anatase titania architectures for high-efficiency dye-sensitized solar cells. *J. Am. Chem. Soc.* **2014**, *136* (17), 6437.
- (54) Zaban, A.; Greenshtein, M.; Bisquert, J. Determination of the electron lifetime in nanocrystalline dye solar cells by open-circuit voltage decay measurements. *ChemPhysChem* **2003**, *4* (8), 859.

(55) Kim, C.; Suh, S.; Choi, M. J.; Kang, Y. S. Fabrication of SrTiO₃-TiO₂ heterojunction photoanode with enlarged pore diameter for dye-sensitized solar cells. *J. Mater. Chem. A* **2013**, *1* (38), 11820.

(56) Sun, H.; Pan, L.; Piao, X.; Sun, Z. Long afterglow SrAl₂O₄:Eu,Dy phosphors for CdS quantum dot-sensitized solar cells with enhanced photovoltaic performance. *J. Mater. Chem. A* **2013**, *1* (21), 6388.

(57) Li, Y.; Yao, B.; Lu, Y.; Li, B.; Gai, Y.; Cong, C.; Zhang, Z.; Zhao, D.; Zhang, J.; Shen, D.; Fan, X. Valence-band offset of epitaxial ZnO/MgO(111) heterojunction determined by X-ray photoelectron spectroscopy. *Appl. Phys. Lett.* **2008**, *92* (19), 192116.

(58) Yi, W. K.; Jeong, T.; Yu, S. G.; Heo, J.; Lee, C.; Lee, J.; Kim, W.; Yoo, J. B.; Kim, J. Field-emission characteristics from wide-bandgap material-coated carbon nanotubes. *Adv. Mater.* **2002**, *14* (20), 1464.

(59) Tang, R.; Yin, L. Enhanced photovoltaic performance of dye-sensitized solar cells based on Sr-doped TiO₂/SrTiO₃ nanorod array heterostructures. *J. Mater. Chem. A* **2015**, *3* (33), 17417.

(60) Baker, D. R.; Kamat, P. V. Photosensitization of TiO₂ nanostructures with CdS quantum dots: particulate versus tubular support architectures. *Adv. Funct. Mater.* **2009**, *19* (5), 805.

(61) Lee, B.; Kim, J.; Lee, S.; Hwang, T.; Nam, S.; Choi, H.; Kim, K.; Kim, J.; Park, B. Oriented hierarchical porous TiO₂ nanowires on Ti substrate: evolution of nanostructures for dye-sensitized solar cells. *Electrochim. Acta* **2014**, *145*, 231.

(62) Liu, Y.; Zhang, M.; Jiang, Y.; Xia, Y.; Sun, W.; Zhao, X. General strategy to construct hierarchical TiO₂ nanorod arrays coupling with plasmonic resonance for dye-sensitized solar cells. *Electrochim. Acta* **2015**, *173*, 483.